IOP Publishing Journal of Physics B: Atomic, Molecular and Optical Physics
J. Phys. B: At. Mol. Opt. Phys. **52** (2019) 155004 (9pp) https://doi.org/10.1088/1361-6455/ab29aa

Simulations of Majorana spin flips in an antihydrogen trap

M A Alarcón[1], C J Riggert[2] and F Robicheaux[3]

[1] Departamento de Física, Universidad de Los Andes, Bogotá, Colombia
[2] Homer L. Dodge Department of Physics and Astronomy, The University of Oklahoma, Norman, OK 73019, United States of America
[3] Department of Physics and Astronomy, Purdue University, West Lafayette, IN 47907, United States of America

E-mail: robichf@purdue.edu

Received 2 April 2019, revised 13 May 2019
Accepted for publication 13 June 2019
Published 18 July 2019

Abstract

The properties of antihydrogen ($\bar{\mathrm{H}}$) have, thus far, been probed at magnetic fields of ∼1 T. It may be fruitful to perform some of these measurements at magnetic fields approaching 0 T. In this case, there could occur zeros in the magnitude of the B-field. The number and properties of the magnetic field zeros are investigated. For typical magnetic field geometries in $\bar{\mathrm{H}}$ traps, the zeros will occur as two groups of 5 closely spaced points instead of as a single point. Except in special cases, results from calculations show that these 10 zeros can be treated as independent sources of spin flip probability. Although the behavior of Majorana spin flip near higher order zeros should not be important in the $\bar{\mathrm{H}}$ traps, the probability for spin flip is calculated for the case of a quadratic zero. Finally, results are presented for a simple model of how magnetic field zeros would affect the trapped population of $\bar{\mathrm{H}}$.

Keywords: antihydrogen, Majorana, spin flip

(Some figures may appear in colour only in the online journal)

1. Introduction

More than 30 years ago, an effort was started to measure properties of the antihydrogen ($\bar{\mathrm{H}}$) atom with the goal of comparing them with their matter counterpart [1]. Because the properties of H and $\bar{\mathrm{H}}$ should be exactly the same by the CPT theorem, any difference would represent a fundamental discovery [2]. It is very difficult to generate any neutral antimatter atom or molecule beyond $\bar{\mathrm{H}}$ which means it is fortunate that so many properties of H are known to ultrahigh precision. In 2002, cold $\bar{\mathrm{H}}$ was experimentally formed at CERN [3, 4]. In 2010, the ALPHA collaboration trapped $\bar{\mathrm{H}}$ [5] and within a year [6] demonstrated that the $\bar{\mathrm{H}}$ could be held for an extensive time, sufficient for precision measurements. To date, only the ALPHA collaboration has measured any property of the $\bar{\mathrm{H}}$ atom although several groups are attempting to measure various properties. Examples of precision measurements include the hyperfine splitting of the $1S$ states [7, 8], the charge of the $\bar{\mathrm{H}}$ [9, 10], the energy difference between the $1S$ and $2S$ states [11, 12], and the Lyman-α transition [13]. Extensions of these measurements could lead to accurate determination of other parameters. For example, a more accurate measurement of the Lyman-α transition would give the Lamb shift or the measurement of another narrow linewidth transition (e.g. $2S$–$4S$) would allow the determination of the antiproton radius and the $\bar{\mathrm{H}}$ Rydberg constant.

The $\bar{\mathrm{H}}$ ground state has 4 non-degenerate levels in a magnetic field. By convention these are labeled $1Sa$, $1Sb$, $1Sc$, $1Sd$ from lowest to highest energy, see figure 1 of [7]. The $1Sa$, $1Sb$ states have decreasing energy with increasing B and, thus, are high field seeking states. Since magnetic traps are constructed from a spatially varying $B = |\vec{B}|$ where there is a minimum B in all three directions, atoms in these two states are expelled from a magnetic trap. The $1Sc$, $1Sd$ states have increasing energy with increasing B and can be trapped. Above ∼0.1 T, the states are effectively two pairs of states with a magnetic moment approximately that of a free electron giving a slope of $(dE/dB)/k_B \simeq 2/3$ K/T. For small magnetic fields (less than ∼0.01 T), the states are more accurately represented as hyperfine eigenstates with an $F = 0$ state

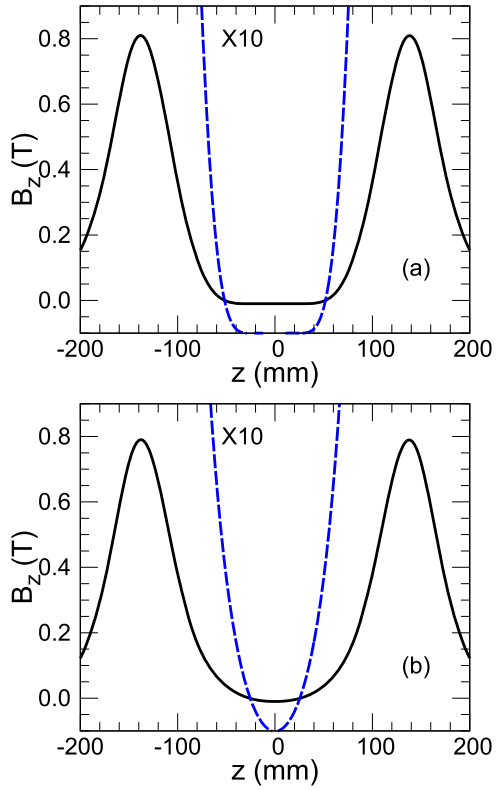

Figure 1. B_z on the trap axis as a function of the axial position. $z = 0$ corresponds to the trap center. Figure 1(a) is from the superposition of 5 mirror coils to flatten the region near $z = 0$. The dashed (blue) line is $10 \times B_z$. Figure 1(b) is from the superposition of 2 mirror coils and leads to a quadratic B_z as a function of z near the center. The dashed (blue) line is $10 \times B_z$. In both cases, the minimum B_z on axis was chosen to be $\simeq -0.01$ T.

1420 MHz below the $F = 1$ states. For small B-field, the $F = 1$ state is split to $M_F = 1, 0, -1$ in increasing order of energy. The $M_F = 0, -1$ are the states that adiabatically connect to the trappable states.

Within the past few years, the ALPHA collaboration has successfully performed several high precision measurements as enumerated in the first paragraph. The cylindrical trapping volume is a tube of length ∼25 cm and radius ∼2 cm. We will denote motion along the axis to be axial motion represented by z while the radial or angular motions will be represented by x, y. Measurements in this trap have taken place in magnetic fields of ∼1 T which forces a comparison between the measured $\bar{\text{H}}$ transition frequencies and *calculated* frequencies using the known properties of the positron and antiproton (e.g. masses, charges, and magnetic dipole moments). If the magnetic field were smaller, then some of the terms in the calculation of transition frequencies become irrelevant. As an example, the diamagnetic shift of the $1S$–$2S$ frequency would be less than 0.4 Hz for $B = 1$ mT [14]. As another example, the shift in energy due to the motional Stark effect was estimated to be ∼300 Hz in a 1 T field [14] but would be much less than 1 Hz in a 1 mT field since the shift is proportional to B^2. This suggests that the path to, for example, ∼1–10 Hz accuracy will be for the experiments to occur at smaller magnetic field.

One of the difficulties of working at a smaller B-field is that it might accidentally go to zero. In this case, the two trapped states, $M_F = 0, -1$, could suffer a Majorana spin flip if the $\bar{\text{H}}$ passes too close to a B-field zero [15–17]. The Majorana spin flip occurs because the body frame direction of the B-field changes more rapidly than the precession frequency when passing near the zero. For $\bar{\text{H}}$, the situation is somewhat complicated because the energies of the $F = 1$ state are not exactly $-\mu B M_F$. However, for the size of B where the spin flip is possible, the linear dependence of the energy on B is good enough to obtain accurate spin flip cross sections. The main complicating factor for traps like that in the ALPHA device is that there is more than one zero and the zeros can be closely spaced; depending on the parameters, 5 zeros can be separated by less than 1 mm. This special condition warrants an investigation of the physics of spin-flip in this type of trap.

This paper is organized as follows. Section 2 gives the possible forms of the B-field near the zeros. Section 3 gives analytic expressions for the spin flip cross section and rate which are accurate when the zeros are separated. Section 4 contains a comparison between the analytic approximation to the cross section and a fully numerical result; conditions are given for when the analytic approximation is accurate. Section 5 contains results for how the spin flip affects the energy distribution of trapped $\bar{\text{H}}$s. There is a short conclusions section, section 6. Section appendix is a short appendix that, for completeness, gives the derivation of the spin flip cross section for an isolated zero.

2. Form of $\vec{B}$ near zeros

For the Majorana spin flip process, the velocity of the $\bar{\text{H}}$ and the variation of the B-field near $|\vec{B}| = 0$ determines the spin flip probability. Away from the zero, the $\bar{\text{H}}$ magnetic moment adiabatically follows the magnetic field direction. To get a sense of the relevant scales, the precession of the positron spin is ∼30 MHz at 1 mT. Since only $\bar{\text{H}}$s with kinetic energy less than $\sim 1/2$ K are trapped, their speed is a few 10's m s^{-1}. At 1 mT, the $\bar{\text{H}}$ travels ∼1 μm during one precession period. The spatial variation of the magnetic field near a zero is ∼1 T m^{-1}. Taking the change in B during one precession period to be ∼10× smaller than B suggests that only regions where the magnetic field is less than ∼0.01 mT are important for spin flip. To be conservative, we investigated cases up to ∼0.1 mT.

To obtain an idea of how many and where the magnetic zeros appear, we numerically found the zeros for the magnetic field trap used in [8, 11–13] but shifted the uniform B_z from the solenoid so that B_z was slightly negative, $B_z = -0.01$ T, in the central region instead of ∼1 T. A schematic drawing of the trap is in any of these papers. Changing the B-field in this way is probably not the method that will be pursued by ALPHA because the currents in the mirror coils and the octupole coil will almost certainly be changed as well. Since these changes are not known, we opted for the simplest

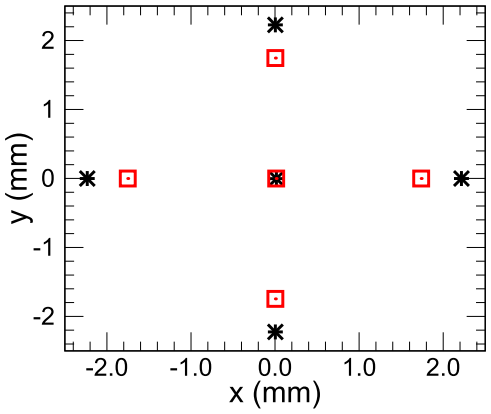

Figure 2. Positions of the magnetic field zeros (at $z < 0$) for the magnetic fields depicted in figure 1 using the full model of the ALPHA trap. For simplicity in the discussion below, both sets of zeros have been rotated by 22.5° clockwise from the coordinates in the ALPHA trap. The black asterisks are for the B-field in figure 1(a) while the red squares are for the B-field in figure 1(b). For the asterisks, the central zero is actually $\simeq$16 μm off the axis and is at a slightly shifted axial position ($z = -51.84$ mm) compared to the off axis zeros ($z = -51.96$ mm). For the squares, the central zero is actually $\simeq$14 μm off the axis and is at a slightly shifted axial position ($z = -25.53$ mm) compared to the off axis zeros ($z = -25.57$ mm).

change that would lead to zeros of the B-field. Specific values (for example, the exact z-position of the zeros) will differ somewhat from future experiments but none of the general features will be affected. The calculations for the data plotted in figures 1 and 2 were done using a model of the coils in the ALPHA trap. This model consists of a series of small, straight current segments which are used with the Biot–Savart Law to give the B-field by superposition. For example, the coil that gives the octupole field is approximated as 17 329 line segments. These models contain all of the imperfections that are known about the actual coils. For example, the model of the ALPHA octupole coil gives a small B_z on axis whereas an idealized octupole field has $B_z = 0$ everywhere.

Mirror coils provide the axial, z, confinement while an octupole coil provides confinement in x, y. The radius of the trap is approximately 22 mm. The on axis B_z is shown in figures 1 where the trapping region is between the B_z-maxima near $z = \pm 138$ mm. In both cases, the outer two coils give a large positive B_z on axis leading to the maxima. In figure 1(a), the middle 3 mirror coils have opposite current (bucked) to the outer coils giving a flattened B-field in the central region. This flattening is desirable because it increases the precision of the spectroscopic measurements and leads to a larger resonance region for the transitions whose frequencies are shifted by B. A nearly uniform B-field along z sets the overall size of the on axis field. The octupole field is nearly zero on axis but plays a large role off axis.

The $10 \times B_z$ in figure 1 makes clearer the two axial positions where the B-field is near 0. In figure 1(a), there is a group of zeros near $z = -52$ mm and another near $z = 52$ mm while they are near $z = -25.5$ mm and 25.5 mm in figure 1(b). Figure 2 shows the x, y positions of the zeros near $z = -52$ mm (case a) and near $z = -25.5$ mm (case b). In both cases, the zeros have been rotated by 22.5° clockwise for simplicity in the discussion below. There is one zero nearly on axis and 4 that are at nearly the same radius and separated by 90°. The off axis zeros near $z = 52$ mm (case a) and $z = 25.5$ mm (case b) are rotated by approximately 45° from those shown in figure 2. Without the octupole field, there is only one zero and it is nearly on axis. The combination of the octupole field and the radial component of the magnetic field from the mirrors lead to the 4 off axis zeros. The slight shift of the central zero from the axis is due to the imperfections of the model of the ALPHA octupole coil.

The form of the magnetic field near the possible zeros is described in this section for the case of an octupole field in x, y plus a cylindrically symmetric field that varies in x, y, z. This geometry is important for the antihydrogen traps because both ALPHA and ATRAP have this magnetic field structure. For an idealization of either apparatus, there is an octupole magnetic field that increases with the radial distance from the center of the trap but whose magnitude has no dependence on the axial coordinate. There will also be a cylindrically symmetric magnetic field with a z-dependence on axis which is a low power, e.g. z^1. Two or more mirror coils can generate axially confining fields that are proportional to z^2 near the minimum or higher power (e.g. z^4 or z^6) when using 5 mirror coils as in ALPHA.

This idealization of the magnetic field is accurate away from the trap walls and in the region where the B-field is near its minimum value. The octupole field seriously deviates from the idealization only near the end of the octupole coils and near the walls ($r \simeq 22$ mm), but the zeros discussed below are always within the central half of the trap and far from the walls, see figure 2 and the caption. The B-fields from the mirrors only deviate from cylindrical symmetry due to the leads or manufacturing imperfections. Thus, the deviations from the ideal case should only lead to small linear terms near the zero which will only slightly modify the variation of the magnetic field. We compared our calculations of spin flip probability using the idealization to those using a full model of all of the ALPHA coils and found only negligible differences once the positions of the zeros were matched.

2.1. Octupole magnetic field

We will approximate the octupole field with the form

$$\vec{B}_o(x, y, z) = \frac{B_w}{r_w^3}(-x^3 + 3xy^2, -y^3 + 3yx^2, 0)$$
$$= \frac{B_w r^3}{r_w^3}[-\hat{e}_r \cos(4\phi) + \hat{e}_\phi \sin(4\phi)], \qquad (1)$$

where r_w is the radius of the trap wall, B_w is the magnitude of the octupole field at r_w, $r^2 = x^2 + y^2$, $\hat{e}_r = \hat{e}_x \cos(\phi) + \hat{e}_y \sin(\phi)$, and $\hat{e}_\phi = -\hat{e}_x \sin(\phi) + \hat{e}_y \cos(\phi)$. This octupole field has the property $|\vec{B}_o| = (r/r_w)^3 B_w$. The form of the octupole field in equation (1) will give zeros *that are rotated* from those of the ALPHA coil but matches those shown in figure 2; this rotation has no effect on the probability for a Majorana spin flip when averaged over all possible trajectories from trapped $\bar{\text{H}}$s. We have

chosen this form, instead of that rotated to match the ALPHA octupole, to simplify the analysis below.

In all of the calculations below, we use $B_w/r_w^3 = 1.375 \times 10^5\ \mathrm{T\,m^{-3}}$ which is a typical value used in ALPHA experiments.

2.2. Octupole plus linear variation

The magnetic field which is cylindrically symmetric and has linear spatial dependence is

$$\begin{aligned}\vec{B}_c &= \frac{B_1}{L}(x,\, y,\, -2(z - z_0)) \\ &= \frac{B_1}{L}[r\hat{e}_r - 2(z - z_0)\hat{e}_z],\end{aligned} \tag{2}$$

where $-2B_1/L$ is the slope of B_z on the axis at the zero which is at $(0,\, 0,\, z_0)$.

The zeros of the total magnetic field are the positions where all components of $\vec{B}_o + \vec{B}_c$ are zero. Since the octupole field has no z-component, all of the zeros are where $B_{c,z} = 0$. This means all of the zeros have $z = z_0$. From the caption of figure 2, this is a good approximation to the actual B-field where the differences in the z-position of the zeros are less than $\simeq$0.1 mm. The off axis zeros can be found by setting the coefficient of $\hat{e}_\phi$ and $\hat{e}_r$ separately equal to 0. Since the cylindrically symmetric field, $\vec{B}_c$, does not have a $\hat{e}_\phi$ component, this conditions sets the angles of the zeros from $\sin(4\phi_0) = 0$: $\phi_0 = n\pi/4$ with $n = 0,\, 1,\, 2,\, ...,\, 7$. Lastly, the coefficient of the $\hat{e}_r$ gives

$$-\frac{B_w}{r_w^3}\cos(4\phi_0)r_0^3 + \frac{B_1}{L}r_0 = 0 \tag{3}$$

which can only be zero if $\cos(4\phi_0) > 0$ when $B_1/L > 0$. This means only 4 of the angles allowed by the $\hat{e}_\phi$ condition give zeros for the $\hat{e}_r$ condition: $\phi_0 = n\pi/2$ with $n = 0,\, 1,\, 2,\, 3$. If $B_1/L < 0$, then the allowed angles are rotated by 45° from the values for $B_1/L > 0$. This feature matches that in the ALPHA B-field. At each of these angles, the radius is the same value

$$r_0 = \sqrt{\frac{B_1 r_w^3}{B_w L}}. \tag{4}$$

These zeros have the same properties as those from the actual B-field: the off axis zeros have nearly the same radius and are separated by 90°. As described in section 2.1, the angles do not match those in the ALPHA trap because of the choice of orientation of the octupole B-field (chosen for simplicity of the resulting analysis).

To give an idea of sizes, the off axis zeros in figure 2 for the case of figure 1(a) are at $r_0 \simeq 2.225 \times 10^{-3}$ m. Using $B_w/r_w^3 = 1.375 \times 10^5\ \mathrm{T\,m^{-3}}$ from the previous section gives $B_1/L = 0.681\ \mathrm{T\,m^{-1}}$.

For the Majorana spin flip, the variation of $\vec{B}$ in the neighborhood of a zero is important. The spatially linear variation $(x,\, y,\, z) = (x_0 + \delta x,\, y_0 + \delta y,\, z_0 + \delta z)$ has the form

$$\vec{B} = \frac{B_1}{L}(\delta x,\, \delta y,\, -2\delta z) + O(\delta^3) \tag{5}$$

for the on axis zero where $O(\delta^3)$ indicates the correction is cubic in the position change. For the off axis zero at $\phi_0 = 0$ (i.e. on the x-axis), a Taylor series expansion gives

$$\vec{B} = -\frac{2B_1}{L}(\delta x,\, -2\delta y,\, \delta z) + O(\delta^2) \tag{6}$$

which has the same form as for the central zero except with a rotated coordinate system and double the slope. All of the off axis zeros have these properties: same form, double the slope of the central zero, and rotated coordinate system.

An important question is whether the zeros will give independent spin flip probabilities for most trajectories or whether the nearness of other zeros will affect the spin flip process. As will be shown in section 4, the zeros give independent contributions to the cross section as long as the separation is larger than (approximately) the square root of the spin flip cross section. The zeros give independent spin flip probabilities at large B_1/L since the separation increases with increasing B_1/L while the cross section decreases. The simulations discussed below show where this approximation gives good results and where it is poor.

2.3. Octupole plus quadratic variation

The magnetic field which is cylindrically symmetric and has quadratic spatial dependence is

$$\begin{aligned}\vec{B}_c &= (0,\, 0,\, B_0) + \frac{B_2}{L^2}\left(-xz,\, -yz,\, z^2 - \frac{1}{2}r^2\right) \\ &= \left(B_0 + \frac{B_2}{L^2}\left[z^2 - \frac{1}{2}r^2\right]\right)\hat{e}_z - \frac{B_2}{L^2}rz\hat{e}_r,\end{aligned} \tag{7}$$

where the on axis minimum of B_z is B_0 at $z = 0$ and B_2/L^2 is half the curvature of the B-field on axis. When only the outer coils make the magnetic trap (e.g. figure 1(b)), the $B_2/L^2 \sim 15\ \mathrm{T\,m^{-2}}$. When the field is flattened as in figure 1(a), there can be inadvertent minima when attempting to obtain a flattened B-field with $B_2/L^2 \sim 1\ \mathrm{T\,m^{-2}}$ or somewhat smaller.

There can only be zeros on axis if $B_0 < 0$ and they are at $z_0 = \pm\sqrt{-B_0L^2/B_2}$ and $r_0 = 0$. The off axis case is a bit more complicated. The $\hat{e}_\phi$ condition still gives $\sin(4\phi_0) = 0$: $\phi_0 = n\pi/4$ with $n = 0,\, 1,\, 2,\, \ldots,\, 7$. The $\hat{e}_r$ condition gives

$$-\frac{B_2}{L^2}r_0z_0 - \frac{B_w}{r_w^3}r_0^3\cos(4\phi_0) = 0 \tag{8}$$

which restricts $\phi_0 = n\pi/2$ with $n = 0,\, 1,\, 2,\, 3$ if $z_0 < 0$ and $\phi_0 = n\pi/4$ with $n = 1,\, 3,\, 5,\, 7$ if $z_0 > 0$. These relations explain why the off axis zeros were rotated by 45° in the actual magnetic field associated with figures 1. This also gives the relationship $r_0^2 = \mathcal{L}|z_0|$ with $\mathcal{L} = (r_w^3/B_w)(B_2/L^2)$. The condition from $\hat{e}_z$ gives

$$z_0^2 - \frac{1}{2}\mathcal{L}|z_0| - z_{0,a}^2 = 0, \tag{9}$$

where $z_{0,a}^2 = -B_0L^2/B_2$ is from the on axis zero. There is a small range of cases where there are zeros with positive B_0 but it is less than $\sim 10^{-8}$ T and, therefore, experimentally irrelevant. For $B_0 \leqslant 0$,

$$|z_0| = \frac{\mathcal{L}}{4} + \sqrt{(\mathcal{L}/4)^2 + z_{0,a}^2} \quad \text{and} \quad r_0 = \sqrt{\mathcal{L}|z_0|}, \tag{10}$$

where $z_{0,a}^2 \geqslant 0$.

It is worth considering the sizes of various terms using $B_2/L^2 \sim 10\,\mathrm{T\,m^{-2}}$ and $B_w/r_w^3 \sim 10^5\,\mathrm{T\,m^{-3}}$. The case $B_0 = 0$ is simple giving $|z_0| = (B_2/L^2)/(2B_w/r_w^3)$ and $r_0 = |z_0|/\sqrt{2}$. This gives a z-separation of ~0.1 mm and a similar size for r_0 implying that $B_0 = 0$ might lead to interesting results. However, even relatively small B_0 leads to the approximation in section 2.2 working well. For example, the case in figure 1(b) has zeros separated by 51 mm. As another example, $B_0 = -1$ mT and $B_2/L^2 = 10\,\mathrm{T\,m^{-2}}$ gives a separation in z of 20 mm while changing to $B_0 = -0.1$ mT gives a separation of 6.3 mm. Therefore, only the $B_0 = 0$ case is probably of interest.

2.4. Octupole plus quartic variation

For the flatter potentials (like that pictured in figure 1), the zeros become like the case of well separated linear zeros, section 2.2. For example, in figure 1, the zeros for the case $B_z(0, 0, 0) = -10$ mT gave a separation of ~104 mm while −1 mT gave a separation of ~80 mm. It is likely that imperfections in the magnetic field will mean this case will not be experimentally attainable.

3. Flip cross section and rate: linear zero approximation

As a baseline, the Majorana spin flip probability will be calculated for a single zero. Since all of the zeros, equations (5), (6), have a linear approximation of the form equation (2) (except rotated), we only discuss the spin flip for that case. The time dependent magnetic field at the atom is determined by the motion of the atom which is assumed to be a straight line at constant speed. To simplify the analysis, the origin of the coordinate system is at the zero of the magnetic field. The position of the $\bar{\mathrm{H}}$ is given by

$$\vec{r}(t) = \vec{b} + \vec{v}t, \tag{11}$$

where b is the impact parameter, v is the speed, and we define the time of closest approach as $t = 0$ which means $\vec{b} \cdot \vec{v} = 0$. Since the position linearly depends on time and the magnetic field linearly depends on the position, the magnetic field linearly depends on time. For this case, Landau–Zener type theories can be used to analytically obtain the transition probability between different states [18]. From the probability as a function of $\vec{b}$ and $\vec{v}$, cross sections for particular transitions have been obtained before [16–18]. For completeness, the derivation of the flip probability is given in the section appendix.

For $\bar{\mathrm{H}}$, the upper two energy levels of the $F = 1$ state are the only ones that are trapped in the magnetic field. The upper level is $M_F = -1$ and the next level is $M_F = 0$. The cross section for various flip processes is calculated from the transition probability which is a function of $\vec{b}$ and $\vec{v}$ for a given $\bar{\mathrm{H}}$ speed, v. The derivation of the cross section for one linear zero is given in the section appendix

$$\begin{aligned} \sigma_{1\leftarrow -1} &= \sigma(v) \quad \text{and} \quad \sigma_{0\leftarrow -1} = 2\sigma(v) \\ \sigma_{-1\leftarrow 0} &= 2\sigma(v) \quad \text{and} \quad \sigma_{1\leftarrow 0} = 2\sigma(v), \end{aligned} \tag{12}$$

where $\sigma(v) = \hbar v/(\mu B_1/L)$ with $\mu = 9.28 \times 10^{-24}$ J/T $\simeq k_B\, 2/3$ K/T, the magnetic moment of the positron. This is an interesting result in that the flip rate, $v\sigma$, is proportional to the kinetic energy of the $\bar{\mathrm{H}}$. This trend agrees with the expectation that the atoms that are lost will tend to be the hottest.

For the case of the octupole plus linear variation in z, there were 5 zeros. The 4 off axis zeros had twice the slope as on the central axis. If all 5 zeros give an *independent* contribution to the Majorana flip cross section, the total cross section for the group of 5 will be

$$\begin{aligned} \sigma_{1\leftarrow -1} &= 3\sigma(v) \quad \text{and} \quad \sigma_{0\leftarrow -1} = 6\sigma(v) \\ \sigma_{-1\leftarrow 0} &= 6\sigma(v) \quad \text{and} \quad \sigma_{1\leftarrow 0} = 6\sigma(v), \end{aligned} \tag{13}$$

where $\sigma(v) = \hbar v/(\mu B_1/L)$. For the actual traps, there are two groups of 5 zeros implying the total flip cross sections are double these results.

4. Comparison to numerical

In this section, the spin flip cross section from the numerical solution of the time dependent Schrödinger equation is presented.

The time dependent Schrödinger equation was solved using the Crank–Nicolson method [19]:

$$\vec{\psi}(t + \delta t) = \frac{1 - iH\delta t/(2\hbar)}{1 + iH\delta t/(2\hbar)}\vec{\psi}(t), \tag{14}$$

where the Hamiltonian, H in equation (23), is evaluated at time $t + \delta t/2$. For spin-1, the Hamiltonian is a 3×3 matrix so the solution of this matrix equation is relatively fast.

The somewhat tricky aspect of obtaining the cross section is to determine the fraction of population where M_F has changed. The eigenstates when $\vec{B} = B(\sin\theta\cos\phi, \sin\theta\sin\phi, \cos\theta)$ are

$$\vec{\psi}_{\pm 1} = \begin{pmatrix} \frac{1}{2}(1 \pm \cos\theta)e^{-i\phi} \\ \frac{1}{\sqrt{2}}\sin\theta \\ \frac{1}{2}(1 \mp \cos\theta)e^{i\phi} \end{pmatrix} \quad \vec{\psi}_0 = \begin{pmatrix} -\frac{1}{\sqrt{2}}\sin\theta e^{-i\phi} \\ \cos\theta \\ \frac{1}{\sqrt{2}}\sin\theta e^{i\phi} \end{pmatrix}. \tag{15}$$

When solving the time dependent Schrödinger equation, the magnetic field will start out in one direction and finish in another. We used these equations to start the wave function at the initial time and to project onto the final states. In the calculations, we started the time propagation so that the $\bar{\mathrm{H}}$ is far enough from the zeros that initially the state adiabatically follows the changing direction of $\vec{B}$ and stopped the propagation when this condition was again satisfied.

We found that using equation (11) did not give results that converged well with the starting and final time. The problem is that starting with equation (11) does not adequately account for the slight difference between the adiabatic and actual wave function unless the magnetic field is very large. This causes the calculations to be quite slow because then the wave function needs to be propagated for longer

times *and* the time steps need to be smaller to account for the larger energy splittings. We found that a $\vec{r}(t)$ where the velocity smoothly turned on from 0 to $\vec{v}$ and then smoothly turned back to 0 allowed for accurate calculation of spin flip probabilities with relatively little numerical effort. We used

$$\frac{d\vec{v}_t(t)}{dt} = \frac{\vec{v}}{\tau\sqrt{\pi}}[e^{-(t-t_i)^2/\tau^2} - e^{-(t-t_f)^2/\tau^2}], \qquad (16)$$

where τ is the duration of the turn-on and $d\vec{r}(t)/dt = \vec{v}_t(t)$ for the time dependent position. We then solved the time dependent Schrödinger equation from $t_i - 6\tau$ to $t_f + 6\tau$. As long as τ was much larger than $\hbar/(\mu B)$ with B evaluated at the starting and final time, then the convergence was much faster with respect to t_i, t_f.

For the calculation of the cross section, we used a Monte Carlo sampling of the $\hat{v}$ and $\vec{b}$. The random parameters were chosen as: b^2 randomly chosen with a flat distribution between 0 and $b^2_{\max}$, $\hat{v}$ randomly chosen with a flat distribution on the surface of a unit sphere, and $\hat{b}$ randomly chosen from a flat distribution on the great circle defined by $\hat{v}\cdot\hat{b} = 0$. The cross section for a transition is the average probability for that transition times $\pi b^2_{\max}$. We checked for convergence with respect to $b_{\max}$ and the number of trajectories. The $b_{\max}$ can be estimated from equation (24) by setting $\Gamma > 16/\pi$ for all angles and adding this to the r_0 of the off-axis zeros.

As a test of the program, we solved for the spin flip cross section for the pure linear B-field, equation (2). We found that the cross section only differed from the analytic value, equation (12), due to statistical sampling.

4.1. Octupole plus linear variation

In this section are the numerical results for the case of the octupole plus linearly varying $\vec{B}_c$ described in section 2.2. For this case, we compared the cross section for independent contribution from the 5 zeros, equation (13), to that from a numerical calculation. In the numerical calculation, we ran approximately 200 000 trajectories to obtain adequate statistics for the Monte Carlo cross section.

The case shown in figures 1(a) and 2 (black asterisks) has a linear parameter $B_1/L = 0.681\ \mathrm{T\,m^{-1}}$. Using these parameters and $v = 50\ \mathrm{m\,s^{-1}}$, we found the Monte Carlo result to be the same as equation (13) within the statistical uncertainty. For this case, $\sigma(v) = 8.33\times10^{-10}\ \mathrm{m^2}$.

To understand when to expect the separated zero approximation, equation (13), to fail, we plot the numerically calculated cross sections versus B_1/L in figure 3. As in the approximation in equation (13), we found that the cross sections for $|\Delta M_F| = 1$ were all the same and those for $|\Delta M_F| = 2$ were all the same. We also show the results for the separated zero approximation, equation (13), as a comparison. As can be seen, there starts to be noticeable differences when $B_1/L < 0.03\ \mathrm{T\,m^{-1}}$ for the $|\Delta M_F| = 1$ case. At the lowest B_1/L calculated ($0.01\ \mathrm{T\,m^{-1}}$), the numerical result is more than a factor of 2 smaller than the separated zero approximation. The $|\Delta M_F| = 2$ is better matched by the approximation with substantial difference only for the smallest B_1/L.

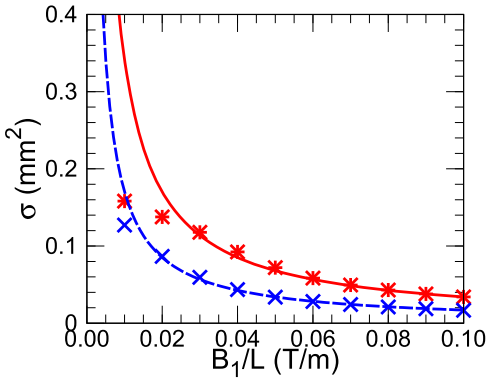

Figure 3. The numerically calculated flip cross sections, $|\Delta M_F| = 1$ (red $*$) and $|\Delta M_F| = 2$ (blue $\times$), compared to the separated zero approximation, equation (13), solid red line and blue dashed line. The statistical uncertainty is less than the size of the symbols.

It seems reasonable that the separated zero approximation will break down when the flip cross section equals πr_0^2 where r_0 is the radius of the off axis zeros, equation (4). For the parameters in this section, this condition gives $B_1/L \sim 0.022\ \mathrm{T\,m^{-1}}$ for the $|\Delta M_F| = 1$ case and $B_1/L \sim 0.015\ \mathrm{T\,m^{-1}}$ for the $|\Delta M_F| = 2$ case. These values are reasonably close to where the differences begin to appear in figure 3. For the $|\Delta M_F| = 1$ case, this condition is $B_1/L = \sqrt{6\hbar v B_w/(\mu r_w^3)}$ and is $\sqrt{2}$ smaller for the $|\Delta M_F| = 2$ case. Experimental control of magnetic fields at this level is possible [8, 12].

4.2. Octupole plus quadratic variation

For this section, we will consider the cases where $1\ \mathrm{T\,m^{-2}} \leqslant B_2/L^2 \leqslant 10\ \mathrm{T\,m^{-2}}$ which is a reasonable range for the $\bar{\mathrm{H}}$ traps. The case of an octupole field plus quadratic cylindrical field, equation (7), has 3 situations worth considering for these parameters: $B_0 > 0.025$ mT, $B_0 = 0$ T, and $B_0 < -0.05$ mT.

The case $B_0 > 0.025$ mT is the simplest. The cross section is, within numerical errors, consistent with 0. The spin can adiabatically follow the changing direction of $\vec{B}$ for this case. We did not test how small can B_0 be before the cross section is non-negligible since 0.025 mT is already below the accuracy for the experimental values of trap parameters.

The next simplest case is $B_0 < -0.05$ mT. In this situation, there are two groups of 5 zeros near $|z_0| \simeq \sqrt{-B_0L^2/B_2} > 1.6$ mm. In this case, the B-field in the neighborhood of the zeros is approximately that of the linear variation case with $B_1/L \simeq z_{0,a}B_2/L^2 = \sqrt{-B_0B_2/L^2}$. In this limit of B_0, the zeros are relatively separated so the approximation in equation (13) can be used. For this case, the 10 zeros sum to give cross sections

$$\begin{aligned} \sigma_{1\leftarrow-1} &= 6\sigma(v) \quad \text{and} \quad \sigma_{0\leftarrow-1} = 12\sigma(v) \\ \sigma_{-1\leftarrow0} &= 12\sigma(v) \quad \text{and} \quad \sigma_{1\leftarrow0} = 12\sigma(v), \end{aligned} \qquad (17)$$

where $\sigma(v) = \hbar v/(\mu\sqrt{-B_0B_2/L^2})$. The numerical results are compared to this approximation in figure 4. As with the comparison in figure 3 for the linear zero, the agreement between the separated zero approximation and the numerical

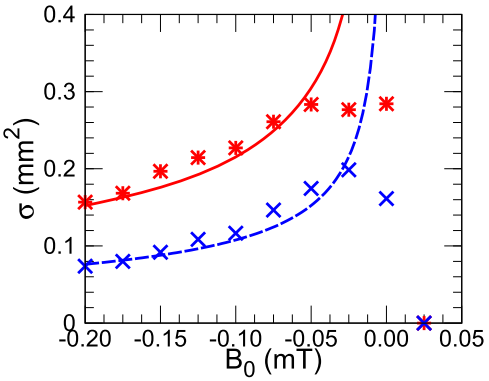

Figure 4. The numerically calculated flip cross sections, $|\Delta M_F| = 1$ (red $*$) and $|\Delta M_F| = 2$ (blue $\times$), compared to the separated zero approximation, equation (17), solid red line and blue dashed line. The statistical uncertainty is less than the size of the symbols.

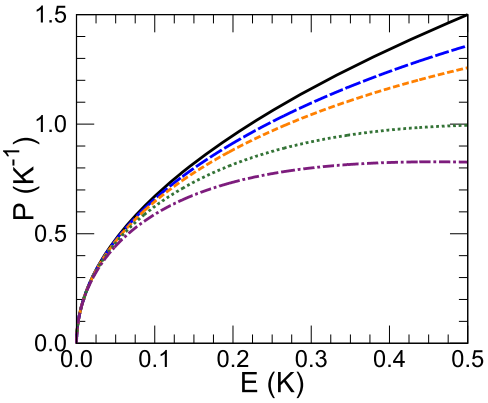

Figure 5. The energy distribution of $\bar{\mathrm{H}}$s after different amounts of interaction with B-field zeros. Both the $M_F = 0$ and -1 states start with the distribution given by the black solid line. At the time when 10% of the $\bar{\mathrm{H}}$s have been lost, the $M_F = -1$ distribution is the dashed (blue) line and the $M_F = 0$ distribution is the short dashed (orange) line. At the time when 30% of the $\bar{\mathrm{H}}$s have been lost, the $M_F = -1$ distribution is the dotted (green) line and the $M_F = 0$ distribution is the dotted–dashed (purple) line.

result is good until the separation of the zeros is comparable to the square root of the cross section.

The last important range is $B_0 \sim 0$. For this value of B_0, the cross section is finite instead of diverging as in equation (17). The approximate size is that for the independent zeros where the square root of the cross section is comparable to the separation of the zeros (similar to the case in figure 3).

5. Antihydrogen loss model

This section contains results for a simple model calculation for the loss of $\bar{\mathrm{H}}$s from a trap for the conditions of figures 1 and 2. For this case there are 10 well separated zeros and the cross section for the various flip processes are the values in equation (17) with $B_1/L = 0.681$ T m^{-1}.

In the ALPHA experiment, the volume of the trap is $\sim$100 cm^3 and they have demonstrated trapping of $\sim$100 atoms [12, 13, 20]. The rough volume estimate is somewhat smaller than the full trap volume because $\bar{\mathrm{H}}$s can not reach all spatial parts of the trap due to energy constraints. Thus, for absolute numbers we will take the $\bar{\mathrm{H}}$ density to be 1 cm^{-3}. Because the trap depth is only $\sim\frac{1}{2}k_B$K and the $\bar{\mathrm{H}}$s are formed at much higher temperatures, the distribution of atoms is approximately a flat distribution in velocity space within a sphere corresponding to a kinetic energy of $\simeq\frac{1}{2}k_B$K leading to a normalized distribution with respect to speed of $P(v) = 3v^2/v_{\max}^3$. This distribution gives good agreement with measurements [13, 21]. From these parameters, we can estimate the rate for a spin flip process with cross section $\sigma = C\sigma(v)$ with $\sigma(v) = \hbar v/(\mu B_1/L)$ to be

$$\Gamma = \rho\frac{3}{v_{\max}^3}\int_0^{v_{\max}} C v\sigma(v)v^2 dv = \frac{3}{5}\rho v_{\max} C\sigma(v_{\max}), \quad (18)$$

where ρ is the number density of $\bar{\mathrm{H}}$s and $v_{\max} \simeq 91$ m s^{-1} for $KE_{\max} = \frac{1}{2}k_B$K. Using these numbers, the $|\Delta M_F| = 2$ rate (uses $C = 6$) is $\Gamma \simeq 0.83$ s^{-1} and the $|\Delta M_F| = 1$ rate (uses $C = 12$) is twice this value. In the ALPHA experiment, the two trapped states are formed with equal probability so the loss rate is the average of these, $\Gamma \simeq 1.2$ s^{-1}. This suggests that the zeros can not be present for more than a couple 10's of seconds before a substantial fraction of the $\bar{\mathrm{H}}$s are lost.

An important question is how the populations evolve if the zeros are present for a substantial amount of time. This is not completely trivial because the higher energy $\bar{\mathrm{H}}$s are preferentially lost *and* because the zeros mix the two trapped states as well as leading to loss. We solved the coupled rate equations at each velocity for the flat velocity distribution described above with $E_{\max} = \frac{1}{2}k_B$K. The $\bar{\mathrm{H}}$s were started with a flat distribution in velocity and equal probability in the $M_F = 0$ and -1 states: the energy distributions are $P_{-1}(E) = P_0(E) = (3/4)E^{1/2}/E_{\max}^{3/2}$. We then evolved the distributions using the rates from equation (17) with $B_1/L = 0.681$ T m^{-1}. The results are shown in figure 5 for the initial distribution and when 10% and when 30% of the $\bar{\mathrm{H}}$s have been lost. As can be seen, the higher energy $\bar{\mathrm{H}}$s are preferentially lost. Also, the distribution goes from equal population in $M_F = 0$ and -1 to a larger fraction of $M_F = -1$. This is because the loss rate from $M_F = 0$ is larger.

There are two major limitations of the model. The first is that the higher energy $\bar{\mathrm{H}}$s are in, effectively, a spatially larger trap. Although the trapping potential in [8, 11–13] are relatively flat, it is not an infinite square well. This means that the higher energy $\bar{\mathrm{H}}$s will pass by the zeros less often than in the simple model calculation. The second is that the mixing between the different degrees of freedom takes some time which can lead to depletion of certain types of trajectories. Again, this will lead to a somewhat smaller loss rate for the regions of phase space that does not mix quickly. Reference [22] found that the higher energy trajectories tended to mix more quickly which might somewhat counteract the effect of the somewhat larger trap volume at higher energy.

6. Conclusions

A description was given of the type of *B*-field zeros expected in $\bar{\mathrm{H}}$ traps. The octupole magnetic field that gives trapping in the radial direction leads to the case where the zeros will typically be in two groups of 5 zeros with the two groups having a large axial separation. The spacing of the zeros within a group of 5 is proportional to the square root of the slope of the *B*-field on axis and inversely proportional to the octupole strength. The cross section for the Majorana spin flip is proportional to the speed of the $\bar{\mathrm{H}}$ and inversely proportional to the slope of the magnetic field on axis at the *B*-field zero. Interestingly, for typical octupole trapping fields, the cross section is independent of the octupole field strength. Numerical calculation of the spin flip cross section were performed and were compared to analytic expressions for the spin flip cross section. The analytic cross sections are accurate as long as the square of the separation of the zeros is larger than the spin flip cross sections.

The evolution of the trap population was calculated for a simple model. In this model, the $\bar{\mathrm{H}}$s have a flat velocity distribution up to a maximum energy; this maximum energy is the trap depth. This simple model showed that the higher energy $\bar{\mathrm{H}}$s are preferentially lost and that an equal distribution of $M_F = -1$ and 0 states becomes somewhat biased to $M_F = -1$.

The results presented above may be useful in designing a strategy for performing experiments on $\bar{\mathrm{H}}$ with small *B*-fields. For example, since the loss rate for an individual $\bar{\mathrm{H}}$ for typical parameters is $\sim 10^{-2}$ s^{-1} and that the loss rate is highest just after the appearance of the zeros, an experiment might slowly lower the uniform *B*-field until the Majorana spin flips start occurring. At that point, the *B*-field can be increased to the point that the flips stop. As long as this manipulation occurs on a time scale less than a couple 10's of seconds, there will not be a substantial loss of $\bar{\mathrm{H}}$s. Finally, it is possible to use these zeros to diagnose properties of the magnetic field that might be useful in experiments. For example, in a measurement of the effect of gravity on $\bar{\mathrm{H}}$s, it is important to not have a spatial gradient in the vertical direction which can mimic the force from gravity. By comparing the expected and measured positions where the spin flips occur, the size of a spatial gradient in the vertical direction can be diagnosed.

Acknowledgments

MAA was supported by the Purdue University SURF program, CJR was supported by the National Science Foundation under Award No. 1460899-PHY REU program, and FR was supported by the National Science Foundation under Award No. 1806380-PHY.

Appendix

This section gives the derivation of the spin flip cross section for completeness.

Start with the form for the magnetic field, equation (2) with $z_0 = 0$, and the position as a function of time, equation (11). Define the magnitudes v, b and the angles α, β where

$$\vec{v} = v(\sin(\beta), 0, \cos(\beta))$$
$$\vec{b} = b(\cos(\alpha)\cos(\beta), \sin(\alpha), -\cos(\alpha)\sin(\beta)). \quad (19)$$

In this equation, advantage has been taken of the cylindrical symmetry of the magnetic field to define the velocity vector to be in the xz plane. The time dependent magnetic field is then

$$\vec{B}(t) = \frac{B_1 b}{L}(\cos(\alpha)\cos(\beta), \sin(\alpha), 2\cos(\alpha)\sin(\beta)) + \frac{B_1 v}{L}(\sin(\beta), 0, -2\cos(\beta))t. \quad (20)$$

The coordinate system is now rotated so that the term multiplying t is purely in the z-direction and the constant part of B_z is removed by defining $t = 0$ as the time of smallest $|\vec{B}|$:

$$\vec{B}(t) = \frac{B_1 b}{L}\left(\frac{2\cos(\alpha)}{\sqrt{1 + 3\cos^2(\beta)}}, \sin(\alpha), 0\right) + \frac{B_1 v}{L}\sqrt{1 + 3\cos^2(\beta)}(0, 0, 1)t. \quad (21)$$

Lastly, rotate in the xy plane so that $B_y = 0$ to find

$$\vec{B}(t) = \hat{e}_x \frac{B_1 b}{L}\sqrt{\frac{4\cos^2(\alpha)}{1 + 3\cos^2(\beta)} + \sin^2(\alpha)} + \hat{e}_z \frac{B_1 v}{L}\sqrt{1 + 3\cos^2(\beta)}\, t \equiv (B_x, 0, \dot{B}_z t) \quad (22)$$

which defines the size of the transverse magnetic field and the size of the time derivative of the magnetic field along z. The Hamiltonian for the spin system is defined as

$$H = -\frac{\mu}{s\hbar}\vec{B}(t) \cdot \vec{S}, \quad (23)$$

where $s = 1$ for the $F = 1$ case and would be $s = 1/2$ for a spin-$1/2$ system.

We will first treat the more familiar spin-$1/2$ system because there is only one spin flip possibility. Using Landau–Zener formalism [15–18], the spin flip probability for a spin-$1/2$ system would be

$$P_{-1/2\leftarrow 1/2} = e^{-2\pi\Gamma} \quad \text{with} \quad \Gamma = \frac{\mu B_x^2}{2\hbar\dot{B}_z}. \quad (24)$$

To obtain the cross section for the spin flip, the probability needs to be averaged over $\cos(\beta)$ and α and integrated over $2\pi bdb$:

$$\sigma(v) = \frac{2\pi}{4\pi}\int_0^\infty \int_{-1}^1 \int_0^{2\pi} P_{-1/2\leftarrow 1/2}\, d\alpha d(\cos\beta) b db. \quad (25)$$

Perform the integration with respect to bdb first to obtain

$$\sigma(v) = \frac{vL\hbar}{4\pi\mu B_1}\int_{-1}^1 \int_0^{2\pi} \frac{(1 + 3s^2)^{3/2}}{4 - 3(1 - s^2)\sin^2(\alpha)} d\alpha ds, \quad (26)$$

where the transformation of variables $s = \cos\beta$ was used.

Integrating over α gives

$$\sigma(v) = \frac{vL\hbar}{4\pi\mu B_1}\int_{-1}^{1} \pi(1 + 3s^2)ds = \frac{\hbar v}{\mu B_1/L}. \tag{27}$$

The case for spin 1 can be done analytically using a result from [18]. The parameters for the Majorana spin flip can be converted to their parameters:

$$b_1 = -b_3 = -\frac{\mu B_1 v}{L\hbar}\sqrt{1 + 3\cos^2\beta}$$
$$g_1 = g_2 = -\frac{\mu B b}{L\hbar\sqrt{2}}\left(\frac{\cos^2\alpha}{1 + 3\cos^2\beta} + \sin^2\alpha\right)^{1/2} \tag{28}$$

and $b_2 = 0$. This leads to probabilities of the same form as for the spin $1/2$ system so that after integrating over impact parameter and averaging over α, $\cos\beta$, the cross sections have the same form:

$$\sigma_{1\leftarrow -1} = \sigma(v) \quad \text{and} \quad \sigma_{0\leftarrow -1} = 2\sigma(v)$$
$$\sigma_{-1\leftarrow 0} = 2\sigma(v) \quad \text{and} \quad \sigma_{1\leftarrow 0} = 2\sigma(v), \tag{29}$$

where we have only included transitions out of the trapped $M_F = 0, -1$ states.

ORCID iDs

M A Alarcón https://orcid.org/0000-0002-5084-8654
F Robicheaux https://orcid.org/0000-0002-8054-6040

References

[1] Gabrielse G, Rolston S L, Haarsma L and Kells W 1988 Antihydrogen production using trapped plasmas *Phys. Lett.* A **129** 38
[2] Bluhm R, Kostelecky V A and Russell N 1999 CPT and Lorentz tests in hydrogen and antihydrogen *Phys. Rev. Lett.* **82** 2254
[3] Amoretti M E A *et al* 2002 Production and detection of cold antihydrogen atoms *Nature* **419** 456
[4] Gabrielse G *et al* 2002 Background-free observation of cold antihydrogen with field-ionization analysis of its states *Phys. Rev. Lett.* **89** 213401
[5] Andresen G B *et al* 2010 Trapped antihydrogen *Nature* **468** 673
[6] Andresen G B *et al* 2011 Confinement of antihydrogen for 1,000 s *Nat. Phys.* **7** 558
[7] Amole C *et al* 2012 Resonant quantum transitions in trapped antihydrogen atoms *Nature* **483** 439
[8] Ahmadi M *et al* 2017 Observation of the hyperfine spectrum of antihydrogen *Nature* **548** 66
[9] Amole C *et al* 2014 An experimental limit on the charge of antihydrogen *Nat. Commun.* **5** 3955
[10] Ahmadi M *et al* 2016 An improved limit on the charge of antihydrogen from stochastic acceleration *Nature* **529** 373
[11] Ahmadi M *et al* 2017 Observation of the 1S–2S transition in trapped antihydrogen *Nature* **541** 506
[12] Ahmadi M *et al* 2018 Characterization of the 1S–2S transition in antihydrogen *Nature* **557** 71
[13] Ahmadi M *et al* 2018 Observation of the 1S–2P Lyman-α transition in antihydrogen *Nature* **561** 211
[14] Rasmussen C O, Madsen N and Robicheaux F 2017 Aspects of 1S–2S spectroscopy of trapped antihydrogen atoms *J. Phys. B: At. Mol. Opt. Phys.* **50** 184002
[15] Majorana E 1932 Atomi orientati in campo magnetico variabile *Il Nuovo Cimento* **9** 43
[16] Zener C 1932 Non-adiabatic crossing of energy levels *Proc. R. Soc.* A **137** 696
[17] Landau L D 1932 Zur theorie der energieubertragung II *Z. Sowjetunion* **2** 46
[18] Sinitsyn N A, Lin J and Chernyak V Y 2017 Constraints on scattering amplitudes in multistate Landau–Zener theory *Phys. Rev.* **95** 012140
[19] Crank J and Nicolson P 1996 A practical method for numerical evaluation of solutions of partial differential equations of the heat-conduction type *Adv. Comput. Math.* **6** 207
[20] Ahmadi M *et al* 2017 Antihydrogen accumulation for fundamental symmetry tests *Nat. Commun.* **8** 681
[21] Andresen G B *et al* 2011 Confinement of antihydrogen for 1,000 s *Nat. Phys.* **7** 558
[22] Zhong M, Fajans J and Zukor A F 2018 Axial to transverse energy mixing dynamics in octupole-based magnetostatic antihydrogen traps *New J. Phys.* **20** 053003